Applied Catalysis B: Environmental 273 (2020) 119053

Contents lists available at ScienceDirect

Applied Catalysis B: Environmental

journal homepage: www.elsevier.com/locate/apcatb

Manipulating the crystalline morphology and facet orientation of copper and copper-palladium nanocatalysts supported on stainless steel mesh with the aid of cationic surfactant to improve the electrochemical reduction of nitrate and N2 selectivity

Yu-Jen Shih[a,*], Zhi-Lun Wu[a], Chun-Yen Lin[a], Yao-Hui Huang[b], Chin-Pao Huang[c,*]

[a] Institute of Environmental Engineering, National Sun Yat-sen University, Kaohsiung 804, Taiwan
[b] Department of Chemical Engineering, National Cheng-Kung University, Tainan 701, Taiwan
[c] Department of Civil and Environmental Engineering, University of Delaware, Newark, DE 19716, USA

ARTICLE INFO

Keywords:
Nitrate reduction
Electrochemical
Crystalline morphology
N_2selectivity
Copper-palladium nanocatalysts

ABSTRACT

Surfactants, namely, cetyltrimethylammonium chloride, polydiallyldimethylammonium chloride, and benzethonium chloride were used to control the crystal growth of metallic Cu nanoparticles supported on stainless steel mesh electrodes as to improve the selective electrochemical conversion of NO_3^- to non-toxic N_2. Results showed that the Cu(200)/Cu(111) ratio controlled the selectivity of N_2, NO_2^-, and NH_4^+. The K_d value increased from 10% to 30% when the Cu(200)/Cu(111) intensity ratio was decreased 60% to 30%, meaning increase Cu(111) increased N_2 production. Furthermore, the presence of a second metal, namely, Pd increased the N_2 selectivity. The best N_2 yield (X_{N2} = 22%), occurring on monometallic Cu, synthesized with BZT at 1-time CMC was further increased to X_{N2} = 65% over bimetallic $Pd_{0.27}Cu_{0.73}$/SS. The selectivity of nitrite (S_{NO2-}) and ammonium (S_{NH4+}) on Cu/SS were 33.1 and 43.5%, respectively, which were decreased to 0.30 and 34.0%, respectively, on bimetallic $Pd_{0.27}Cu_{0.73}$/SS.

1. Introduction

Inorganic nitrogen, typically nitrate (NO_3^-), nitrite (NO_2^-) and ammonia (NH_3), derived from microbial degradation of organic nitrogen, are essential micronutrients [1]. Anthropogenic activities, such as farmland fertilization, industrial chemical synthesis and manufacturing, and domestic sanitation have contributed a high level of nitrate to natural water systems [2]. Nitrate in drinking water exhibits adverse human health effects upon reduction to nitrite, i.e., metahemoglobinemia, and behaves as a precursor of carcinogenic nitrosamines [3]. Current physical-chemical processes, such as adsorption, ion exchange, reverse osmosis, or electrodialysis are efficient in nitrate removal [4]. However, there are drawbacks such as production of secondary concentrate waste streams, high process and energy cost that limit the applicability of these above methods for treating nitrate containing waters [5]. Microbial reaction can completely convert nitrate to nitrogen byproducts effectively, but biological processes lack the brine disposal capacity [6,7]. Furthermore, sludge production and slow denitrification decreased the effectiveness, specifically, of biological methods when treating highly contaminated water and wastewater [8]. Nitrite contamination of groundwater has been reported worldwide. The European Union (Nitrates Directive - 91/676/EEC) has establish a limit of 50 mg-NO_3^-/L for all freshwaters. Meanwhile, the World Health Organization (WHO) has a regulation of 50 mg-NO_3^- L^{-1} and 3 mg-NO_2- L^{-1} for drinking water. A much lower nitrogen concentration of around 1–2 mg-N L^{-1} can trigger eutrophication in oligotrophic waters [9]. Therefore, green technique capable of achieving high NO_3^- reactivity with high N_2 selectivity is urgently needed to safe guard water quality. Electrochemical process, involving *in-situ* mediation of electrons for direct redox reactions or indirect generation of strong oxidants or reductants, is a powerful technology for the treatment of a wide variety of organic and inorganic pollutants [10–13]. Moreover, use no additional chemicals, electrochemical nitrate removal process consumes less energy, produces almost no sludge and has remarkable environmental compatibility [14,15].

Chemical and electrochemical reduction of NO_3^- over catalysts, such as noble metals (Pd, Pt, Au) and transition metals (Cu, Sn, In, Fe, Ti) have exhibited high NO_3^-removal reactivity and N_2 selectivity

* Corresponding authors.
E-mail addresses: yjshih@mail.nsysu.edu.tw (Y.-J. Shih), huang@udel.edu (C.-P. Huang).

https://doi.org/10.1016/j.apcatb.2020.119053
Received 13 January 2020; Received in revised form 19 April 2020; Accepted 21 April 2020
Available online 05 May 2020
0926-3373/

simultaneously [16–20]. The effectiveness of electrochemical NO_3- reduction, as affected by the step and mechanism of electron transfer, over-potential, and ion capacitive charging, strongly depends on the physical properties of electrode materials [21]. Catalyst nanoparticles (NPs) generally exhibits a variety of surface morphology, e.g., facet, shape, and size, which determines the intrinsic reactivity and selectivity [22]. Electrodeposition conditions, such as pH, metal salt concentration, temperature, and electroplating time, play an essential role on controlling the micromorphology of metallic particles. Surfactant additive, such as sodium dodecyl sulfate (SDS), ascetyltrimethylammonium bromide (CTAB), and polyvinylpyrrolidone (PVP), capping regent inhibiting crystal growth, can manipulate the development of specific crystal facet, thereby affecting the reactivity and selectivity [23–26].

Cu and Cu_2O are electron mediators, more reactive toward nitrogen than other metals [27]. We previously studied the electrochemical treatment of nitrate over Cu/Ni electrode prepared with electrodeless-plating and reported that although the preference of Cu(111) and Cu (200) facets of Cu or Cu_2O was controlled by electroplating duration, which influenced N_2 yield. The mechanism of direct NO_3^- reduction was not different among Cu facets [28], which resulted in the yield of NO_2^-, N_2, and NH_4^+, depending on the extent of overpotential [29].

$$NO_3^- + 2H^+ + 2e^- \rightleftharpoons NO_2^- + H_2O;\ E^o = 0.836\,V\ (vs.\ NHE) \quad (1a)$$

$$2NO_3^- + 12H^+ + 10e^- \rightleftharpoons N_2 + 6H_2O;\ E^\circ = 1.246\,V\ (vs.\ NHE) \quad (1b)$$

$$NO_3^- + 10H^+ + 8e^- \rightleftharpoons NH_4^+ + 3H_2O;\ E^\circ = 0.881\,V\ (vs.\ NHE) \quad (1c)$$

Bimetallic catalysts, especially those metals having strong surface affinity toward hydrogen (Pd, Rh or Ru) are ideal electron promoters and thereby generally exhibit better reduction selectivity than monometallic electrodes [30–32]. Specifically, Pd captured H_{ads} strongly and promoted the indirect NO_3^- reduction via hydrogenation reaction over Pd-Cu and Pd-Sn electrodes [33–36].

$$NO_3^- + 2H_{ads} \longrightarrow NO_2^- + H_2O \quad (2a)$$

$$2NO_3^- + 10H_{ads} + 2H^+ \longrightarrow N_2 + 6H_2O \quad (2b)$$

$$NO_3^- + 8H_{ads} + 2H^+ \longrightarrow NH_4^+ + 3H_2O \quad (2c)$$

In the present work, we will test two hypotheses: (1) metallic catalysts consist of reactive metal in effectively transferring electron for nitrogen compounds, assisted with one hydrogen active metal, will be more efficient than monometallic catalysts in nitrate reduction, and (2) crystal facet plays a role on nitrate reactivity and nitrogen selectivity. To verify the hypotheses, monometallic Cu and bimetallic Pd-Cu electrodes, supported on stainless steel, were fabricated, characterized, and studied for nitrate reduction. The effect of chemical additives on the crystal facet and morphology of electrocatalyst toward improving hydrogen gas evolution in energy research, has been extensively studied [37,38]. Recently, we have studied the effect of roughness of metallic catalysts, through controlling the mode of metal electroplating, on nitrate reduction [32]. Little information is available on the use of surfactants to tailor the crystal growth of Cu nanoparticles as to enhance the electrochemical nitrate reduction and improve nitrogen selectivity. It is further hypothesized that electrochemical deposition conditions, specifically, the type and concentration of surfactant, control the morphology of Cu crystals, which in turn affects the reactivity and selectivity of NO_3^- reduction. Three types of cationic surfactants, namely, cetyltrimethylammonium chloride (CTAC), polydiallyldimethylammonium chloride (PDDA), and benzethonium chloride (BZT) were studied. Cu electrodes, i.e., Cu/SS, were prepared in electrolyte solutions containing cationic surfactants at different concentrations with respect to their critical micelle concentration (CMC). The influence of Cu crystal facet of Cu/SS electrodes on the electron transfer and selective conversion of NO_3^- was evaluated. The Cu/SS electrodes were then decorated with palladium (Pd) at different Pd to Cu atomic ratios to synthesize bimetallic Pd-Cu/SS electrodes. The NO_3^- reduction capability and N_2 yield over Cu/SS and Pd-Cu/SS electrodes were studied. Overall, it was aimed at gaining insights into the mechanisms of selective nitrate reduction as affected by crystal facet.

2. Materials and methods

2.1. Electrochemical plating of Cu/SS and Pd-Cu/SS electrodes

The substrate for Cu deposition was stainless steel (SS) mesh (grade 304, standard wire gauge #40, mesh number = 80 per inch, wire diameter = 0.12 mm), purchased from ESZ Company, Taiwan. The SS mesh was initially degreased with acetone (99.5%, J.T. Baker, USA), acid-etched in 3 M of H_2SO_4 for 10 min, and rinsed with deionized water in ultrasonic bath. The plating bath comprised of 0.5 M of $CuSO_4$•$5H_2O$ (Honeywell, USA) and given concentration of surfactant, with pH being adjusted to 2 using H_3PO_4 (85%, Honeywell, USA). Two surfactants, cetyltrimethylammonium chloride (CTAC, $C_{19}H_{42}ClN$, 96%, Alfa Aesar, USA) and benzethonium chloride (BZT, $C_{27}H_{42}ClNO_2$, 98%, Sigma-Aldrich, USA), with critical micelle concentrations (CMC) of 1.1×10^{-3} and 1.78×10^{-3} M, respectively, and a polyelectrolyte, polydiallyldimethylammonium chloride (in unit of N for dimethylamine group) (PDDA, MW = 240,000, 20 wt% (~1300 meq L^{-1}), Sigma-Aldrich, USA), were selected. Electrochemical plating was conducted with SS and commercial IrO_2/Ti as cathode and anode, respectively, at a constant current of 80 mA cm^{-2}. After Cu plating, the Cu/SS electrode was rinsed with 0.1 M of H_2SO_4 to remove residual salts, and then used as the cathode in bath containing 1×10^{-3} M of $PdCl_2$ (Sigma-Aldrich Co., USA) and 0.25 M of HCl to begin synthesize the Pd-Cu/SS electrodes. All electrodes were dried in vacuum before use.

2.2. Batch electrochemical reduction of nitrate

Batch constant current experiments at 3 mA cm^{-2} was performed to assess the performance of surfactant-modified electrodes in nitrate reduction. The electrochemical reactor (Fig. S1) was constructed with two polymethyl methacrylate (PMMA) plates, intercalated between electrodes and a spacer at a distance of 0.5 cm in between the two electrodes. To minimize ammonia leaking from stripping, the reactor was tightly sealed with a cover, Teflon tape, and grease. Separate experiment was run to assess the loss of ammonia from the reactor (Fig. S1). Results showed that loss of ammonia was less than 7% at pH11 and initial NH_3 concentration of 200 mg-N/L in 5 h, the same duration as all electrochemical nitrate reduction experiments (Figs. 5 and 7). Further, all batch experiments in the present work were performed at pH around 8.5,which was about 1 pH unit below the acidic constant of ammonium ion, i.e., $pK_a = 9.25$. Under such pH condition, cationic ammonium, non-volatile, was the major species (molar fraction ~85%) in the solution. Therefore, it could be assured that the extent of ammonia stripping was insignificant. The synthesized Cu/SS or Cu-Pd/SS was cut into a dimension of $5 \times 5\,cm^2$ (total effective area ~25 cm^2) for use as the cathode. An IrO_2/Ti net of the same dimension as the Cu electrode was used as the anode. The percentage of nitrate removal (R, %), selective nitrogen (S_N, %) and N_2 yield (X_{N2}) were obtained at specific reaction time, *t*, according to the following equations:

$$R(\%) = \frac{C_{NO_3^-,0} - C_{NO_3^-,t}}{C_{NO_3^-,0}} \times 100 \quad (3a)$$

$$S_N(\%) = \frac{C_N}{C_{NO_3^-,0} - C_{NO_3^-,t}} \times 100 \quad (3b)$$

$$X_{N_2} = R \times S_{N_2} = \frac{C_{N_2}}{C_{NO_3^-,0}} \quad (3c)$$

where C_N stands for the concentration of nitrogen products, such as

NH_4^+-N, NO_2^--N, and N_2-N in mol L^{-1}, respectively. S_N represents the amount of nitrogen produced per mass of nitrate reduced, and X_{N2} is the mole of N_2-N formation per mole of initial NO_3^--N.

2.3. Chemical nitrogen analysis and surface characterization of electrode

Electrochemical properties of Cu/SS and Pd-Cu/SS were characterized using potentostat (CHI611C, CH Instruments, Inc., Austin, TX, USA). The counter electrode was IrO_2/Ti and the reference electrode was Hg/HgO/1 M NaOH (E^0 = 0.14 V vs. NHE) (RE-61AP, ALS Co. Ltd., Tokyo, JAPAN). NO_3^- (in KNO_3) was the reacting species (J.T. Baker, USA) in 0.1 M of sodium sulfate solution (Na_2SO_4, Sigma-Aldrich Co., USA). The solution pH was adjusted to a specific value with sodium hydroxide (NaOH, Merck KGaA, Darmstadt, Germany) and sulfuric acid (H_2SO_4, 95%, Sigma-Aldrich Co., St. Lewis, USA).

The analysis of nitrate was based on the colorimetric method (Method 353.2, USEPA). Briefly, nitrate was reduced to nitrite using a copperized cadmium column prior to diazotization of nitrite with sulfanilamide ($H_2NC_6H_4SO_2NH_2$, Sigma-Aldrich Co., USA), followed by coupling with N-(1-naphthyl)-ethylenediamine dihydrochloride (NED, $C_{10}H_7NHCH_2CH_2NH_2$•2HCl, Sigma-Aldrich Co., USA) to obtain the concentration of total oxidized nitrogen (NO_x-N). The concentration of pink azo dye was calibrated spectrophotometrically at 540 nm. Total NO_x measured minus nitrite gave the nitrate nitrogen. Analysis of ammonia was based on the indophenol method at 630 nm according to the Berthelot reaction (Method 350.1, USEPA), in which the ammonia nitrogen reacted with phenoxide ($NaOC_6H_5$•$3H_2O$) and hypochlorite (NaClO) using nitroprusside ($Na_2[Fe(CN)_5NO]$) (Riedel-deHaën AG, Germany) catalyst. A flow injection analyzer (FIA, Lachat's Quik Chem 8500 Series 2, Love land, Colorado, USA) was used to automatically measure the concentration of aqueous nitrogen species (NO_3^--N, NH_4^+-N, NO_2^--N). The detection limit was 0.2 μg L^{-1} for NH_4^+-N, and 0.25 μg L^{-1} for both NO_2^--N and NO_3^--N. Deionized water, purified with a laboratory-grade RO-ultrapure water system (resistivity > 18.18 MΩ cm), was used for the preparation of all solutions.

Scanning electron microscope (SEM, JSM-6700 F, JEOL, Tokyo, Japan) integrated with an energy dispersive spectroscopy (EDS, INCA400, Oxford, UK) was used to assess the morphology and the elemental components of Cu/SS and Pd-Cu/SS electrodes. The crystallographic structure was analyzed by X-ray diffraction (XRD, DX III, Rigaku Co., Tokyo, Japan) operated under the following conditions: Cu Kα source (λ = 1.5406 Å), scan rate = 0.06° s^{-1}, incidence angle = 20-85° (2θ). The chemical state was characterized by X-ray photoelectron spectroscopy (XPS, PHI 5000 VersaProbe, Physical Electronics, Inc., USA) with a monochromatic Al Kα X-ray source (1487 eV).

3. Results and discussion

3.1. Characterization

Fig. 1 shows the micromorphology of surfactant-modified Cu/SS and Pd-Cu/SS observed by SEM. The concentration of surfactant added in the plating bath were in the range of 0.5 × to 10 × CMC for CTAC, 0.5 × to 2 × CMC for BZT, and 0.01 and 0.1 N of amine functional group for PDDA; CMC was the critical micelle formation concentration. Surfactants as additives in different concentrations strongly affected the crystallinity of Cu electrode. The CTAC-modified Cu nanoparticles were well dispersed with an average grain size of 50 nm. The hydrophilic amine head of CTAC was attached to Cu and the hydrophobic tail of 16-C group entered into the aqueous phase, which hindered further grain growth [39]. As the nano-sized Cu particles aggregated, the clusters size increased with increasing CMC (Fig. 1a-d). The positive-charged dimethylamine of PDDA completely leaned on the negative cathode surface, while the polymer chain loops gave rise to a rough and porous Cu deposits on the SS surface, when PDDA concentration increased (Fig. 1e & f). The geometry of Cu nanoparticles was better controlled by the addition of BZT; Cu nanoparticles evolved as vertex-octahedrons at low CMC, suggesting the predominance of {111} facet (Fig. 1g-i) [28]. The vertex-octahedrons capped at high CMC, was similar to those formed in the presence of CTAC, which constrained the evolution of facets and produced nano-crystallites alongside the large crystals. The 1 × CMC BZT-modified Cu/SS was used as the substrate to synthesize Pd-Cu/SS via electro-plating. Fig. S2 shows the EDS elemental mapping of the geomorphology of Pd over the Cu crystals. Metallic Pd nanoparticles did not cover the Cu surface, but nucleated around the boundary of Cu crystals, thereby exposing the specific facets of Cu to the solution (Fig. 1j-l). More Pd aggregates were produced surrounding the crystalline Cu when the plating time was extended.

The XRD patterns of all Cu/SS electrodes prepared in different type and concentration of surfactants were presented in Supplementary Data (Fig. S3). The three major peaks at 2θ 43.3°, 50.4°, and 74.1° were assigned to the ordering planes of Cu(111), Cu(200), and Cu(220), respectively (Fig. 2a). The area ratio of the top two intense peaks, (200)/(111), (which was used as a factor for evaluating the facet effects on reactivity/selectivity in the present study) varied with the type and concentration of surfactants. Furthermore, a new Cu_2O phase was created at 2θ 36.4° and 42.3° assigned to Cu^I(111) and Cu^I(200), respectively, upon the incorporation of Pd. Fig. 2b shows the presence of Pd metal at 2θ 40°, 46.5°, and 68.3° representing the Pd(111), Pd(200), and Pd(220) facets, respectively [40]. The intensity of metallic Cu peaks sharply decreased with increasing Pd plating time (from 1 to 10 min), which implied the corrosion of Cu facets. Since $PdCl_2$ is a relatively strong oxidant (Pd^{2+} + $2e^-$ ⇌ Pd; E° = 0.951 V) in acidic electrolyte, Pd deposition might lead to Cu oxidation via the electrodeless mechanism (i.e., Pd^{2+} + Cu + H_2O → Pd + Cu_2O + $2H^+$; ΔG° = -23.79 kCal). Consequently, the small Cu crystallite seeds aided the accumulation of Pd particles, while a thin and passivating film of cuprous oxide developed on the smooth facets of the large Cu crystals.

Fig. 3a presents XPS spectra of Cu 2p orbital on Pd-Cu/SS electrodes, which clearly showed the formation of Cu_2O over Pd-Cu/SS electrodes. The plating time of Pd strongly affected the oxidation state of Cu; a significant portion of copper on Cu/SS (prepared at 1 × CMC BZT) was in the Cu(II) state at 934.3 eV of Cu $2p_{3/2}$ orbital. Pd loading reduced the Cu(II) signal and increased the Cu(0)/Cu(I) state at 932.3 eV [41]. 245Cathodic plating completely reduced the residual surface Cu(II) ions to Cu(0), whereas Pd plating transformed more Cu (0) to Cu_2O and increased the amount of Pd deposition on Pd-Cu/SS. The Pd $3d_{5/2}$ and Pd $3d_{3/2}$ states that appeared around 335.8 and 341.0 eV, 336.3 and 341.5 eV, 336.9 and 342.2 eV and 338.2 and 343.4 eV were attributed to the species of Pd(0), $Pd(OH)_X$, PdO, and PdO_2, respectively [42,43]. Results in Fig. 3b showed that Pd(OH)x and PdO were transformed to elemental Pd as the plating time increased. Fig. 3c shows the atomic ratio of Pd to Cu on Pd-Cu/SS electrodes. Results shows that $Pd_{0.17}Cu_{0.82}$/SS, $Pd_{0.27}Cu_{0.73}$/SS, and $Pd_{0.49}Cu_{0.51}$/SS were successfully synthesized at 1, 5 and 10 min of plating, respectively.

Fig. 2c shows the correlation between surfactant concentration and Cu facet ratio (200)/(111) of the Cu/SS electrodes. Results indicated that the Cu(200)/Cu(111) ratio increased with increasing CMC of CTAC and BZT, but insignificant variation with respect to PDDA concentration. Accordingly, high surface-energy facets grew faster that the lower ones. The predominance of facet depends on the growth rate of that specific crystal plane. A facet with relatively high surface energy will evolve with a high crystal growth rate in the direction of that facet vector, while facets with low surface energy become predominatedted. In other words, high-energy facet will lost its dominance to low-energy surfaces [44]. For example, if Cu continuously grew in Cu(111) direction with a rate higher than that of Cu(100), then Cu(100) would dominante eventually. Thus, low intensity ratio of Cu(200)/Cu(111) obtained at low surfactant concentration indicated that the surface energy of metallic Cu(200) was higher than that of Cu(111). The

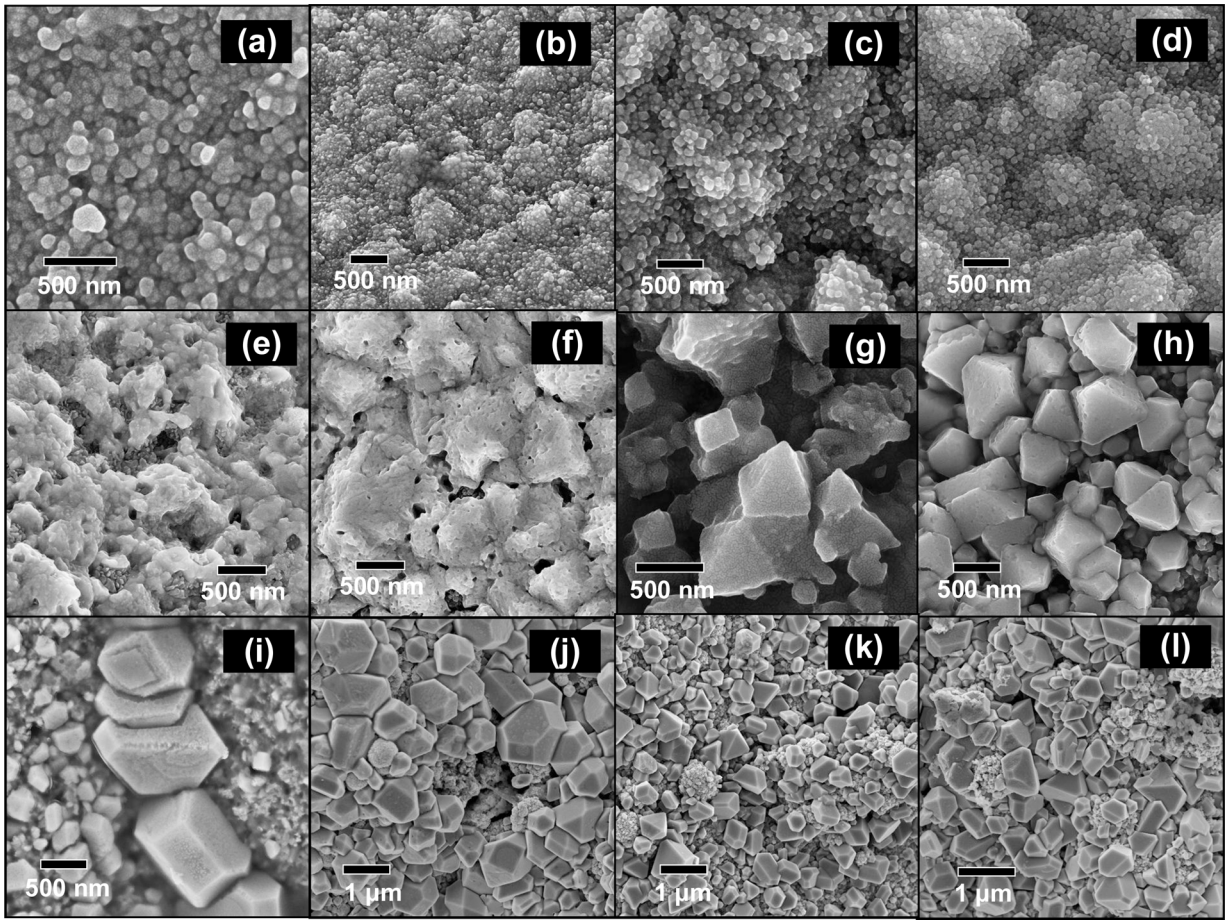

Fig. 1. SEM micromorphology of Cu/SS electrodes synthesized under conditions: $[Cu^{2+}]$ = 0.5 M, current density = 80 mA cm^{-2}, pH 2 (adjusted by H_3PO_4), cathode = stainless steel mesh, anode = IrO_2/Ti in the presence of surfactants: (a) 0.5 × CMC CTAC, (b) 1 × CMC CTAC, (c) 2 × CMC CTAC, (d) 10 × CMC CTAC, (e) 0.01 N PDDA, (f) 0.1 N PDDA, (g) 0.5 × CMC BZT, (h) 1 × CMC BZT(i) 2 × CMC BZT. SEM image of Pd-Cu/SS modified with 1 × CMC BZT and different Pd plating times: (j) 1 min, (k) 5 min, (l) 10 min.

specific adsorption of surfactant on high-energy Cu(200) slowed the crystal growth of Cu(200) when CMC was increased, thereby increased the intensity ratio of Cu(200)/Cu(111). However, the Cu(200)/Cu(111) ratio decreased with increase in Pd loading. The uptake of more Pd^{2+} enabled a higher erosion rate of Cu(111) along the [111] than the [100] direction. That is, Cu_2O crystal was preferentially orientated in the Cu^{I} (111) facet of Pd-Cu composites. (Note that growth results in the exposure of low-energy surfaces, while in contrast etching leads to the formation of high-energy surfaces [45]). Fig. 2d gives the primary grain size, d_S, of Cu particles on Cu/SS and Pd-Cu/SS electrodes determined from the full- width-maximum of Cu(111) and Cu(200) peaks, according to the Scherrer equation. The surfactant concentration did not, but surfactant type did, affect d_S. The d_S of CTAC-modified Cu/SS was 10–15 nm, which was smaller than that of PDDA- and BZT-modified Cu/SS electrodes at average 40 nm and 35 nm, respectively. The crystallographic size of Cu crystals was similar to that observed from SEM images. Results also showed that CTBA inhibited particle growth as polycrystals more significantly than PDDA and BZT. The decrease in the grain size of Cu on Pd-Cu/SS modified with 1 × CMC of BZT was attributed, in part, to the corrosion of Cu by Pd.

3.2. Electrochemical characteristics with respect to nitrate reduction

Fig. 4a gives the voltammetry of metallic Cu on the surfactant-modified Cu/SS electrodes (supporting electrolyte = 0.1 M Na_2SO_4) by cyclically scanning the potential window from +0.1 V to -1.2 V (vs. Hg/HgO). In the anodic direction, the two peak potentials of O_1 and O_2 at -0.2 and -0.05 V, respectively, were results of Cu passivation: $2Cu^{(0)} + H_2O \rightarrow Cu_2O(s) + 2H^+ + 2e^-$ at -0.2 V (O_1), and $Cu_2O(s) + H_2O \rightarrow 2CuO(s) + 2H^+ + 2e^-$ at -0.05 V (O_2) [28]. The reversible current of R_1 peak against the square root of scan rate was used to evaluate the diffusion-limited electron transfer for the Cu°/Cu^{I} redox couple, in which the linear regression yielded the proton diffusion coefficient (D_H) (Supporting data, Fig. S4 & S5). Fig. 4b shows an increase in D_H with increase in Cu(200)/Cu(111) ratio; namely, Cu(200) was more effective than Cu(111) in mediating the electron transfer for the reduction of the oxidized Cu film.

An additional current appeared at the onset potential of around -0.6 V in the nitrate solution, (R_N, Fig. 4c). The peak current at R_N appeared to reflect nitrate concentration, indicating the reduction of surface $Cu^{(I)}$ to $Cu^{(0)}$ and NO_3^- during sweeping the cathode potential. The total current of nitrate reduction was subtracted from the background current of $Cu^{(\circ)}/Cu^{(I)}$ redox to obtain the net current as shown in Fig. S6. According to the Nicholson and Shain equation, the peak current of faradaic reaction (i_p) can be used to estimate the number of electron transfer during NO_3^- reduction: $i_p = 2.99 \times 10^5 n(\alpha)^{1/2} AD^{1/2} C^* v^{1/2}$, where A is the effective area (5 cm^2), v is the scan rate (10 mV s^{-1}) and D is the diffusion coefficient of NO_3^- (e.g., 1.7×10^{-5} cm^2 s^{-1}) [46,47]. The term α is the transfer coefficient of the rate-determining step, estimated by $|E_p - E_{p/2}| = 47.7/\alpha$ (mV) at 298 °C, where $E_{p/2}$ is the potential at $I_{p/2}$. I_p of R_N was linearly plotted versus $C^*\alpha^{1/2}$ (Fig. 4d), which indicated diffusion-controlled NO_3^- reduction. The slope of I_p versus $C^*\alpha^{1/2}$ plot gives the number of electron transfer in the multistep reduction of NO_3^-. Fig. 4e shows that n was positively

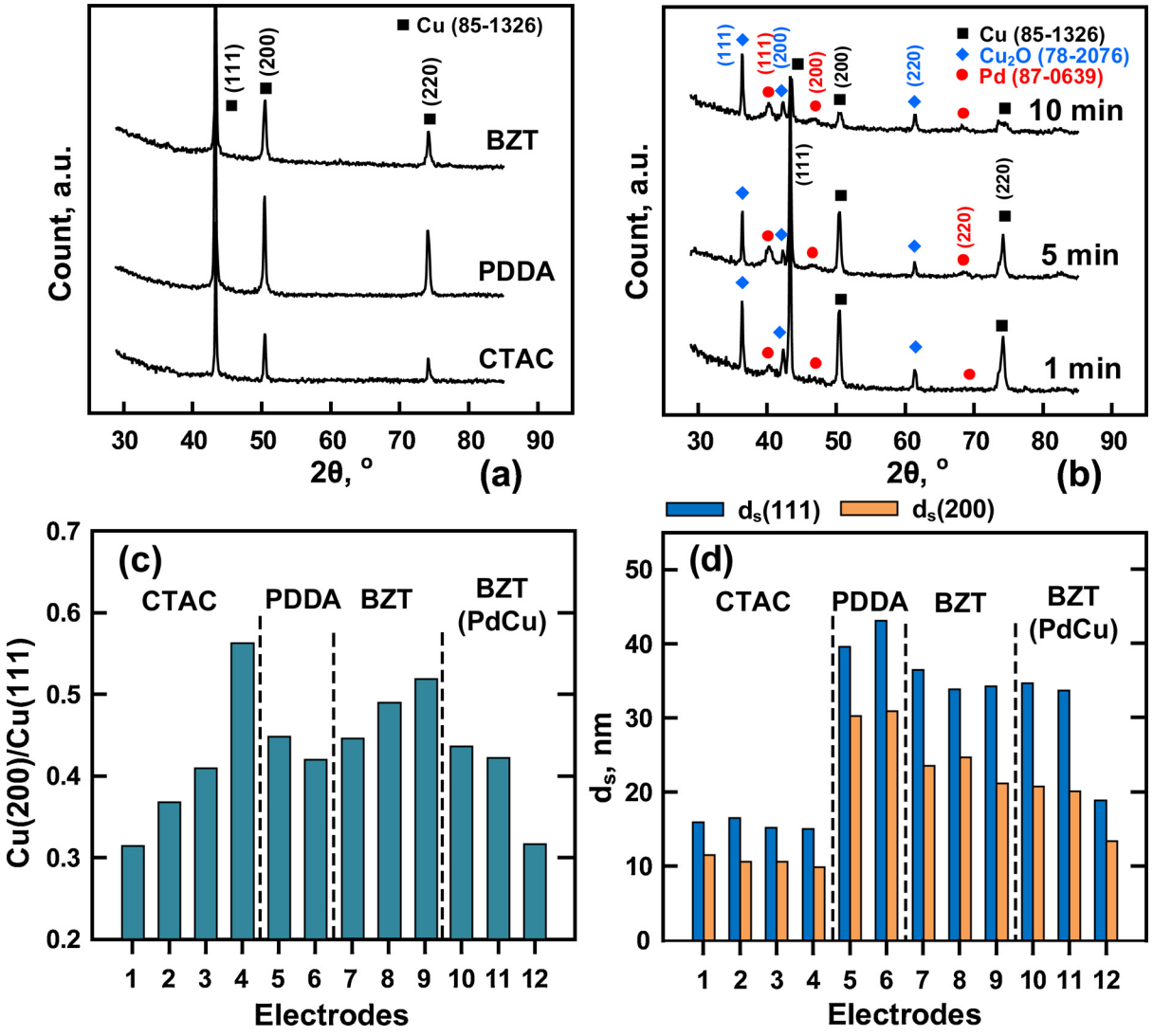

Fig. 2. XRD patterns of (a) Cu/SS electrodes prepared in the presence of 10 × CMC CTAC, 0.1 N PDDA, and 2 × CMC BZT, and (b) Pd-Cu/SS at different Pd plating times. (c) Peak area ratio of Cu(200) to Cu(111) facets and (d) the corresponding crystalline size of surfactants-modified Cu/SS electrodes with: (1) 0.5 ×, (2) 1 ×, (3) 2 ×, (4) 10 × CMC CTAC, (5) 0.01 N, (6) 0.1 N PDDA, (7) 0.5 ×, (8) 1 ×, (9) 2 × CMC BZT, and 1 × BZT modified Cu/SS electrodes with different Pd loadings: (10) $Pd_{0.17}Cu_{0.82}$/SS, (11) $Pd_{0.27}Cu_{0.73}$/SS, and (12) $Pd_{0.49}Cu_{0.51}$/SS.

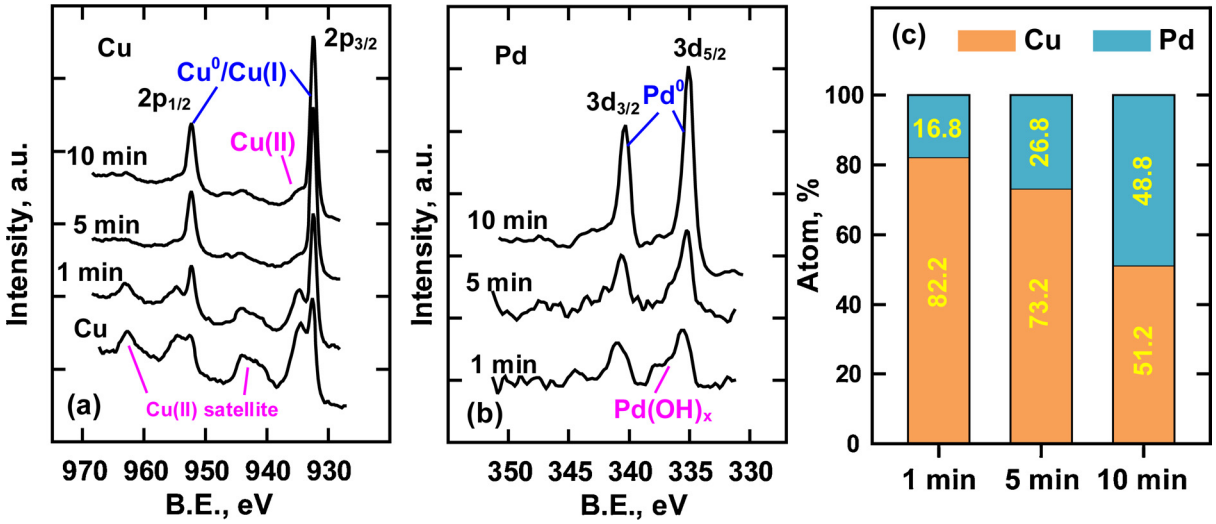

Fig. 3. XPS spectra of (a) Cu 2p, and (b) Pd 3d for Cu/SS and Pd-Cu/SS electrodes at different Pd plating times. (c) Atomic Pd to Cu ratio on Pd-Cu/SS as a function of Pd plating duration.

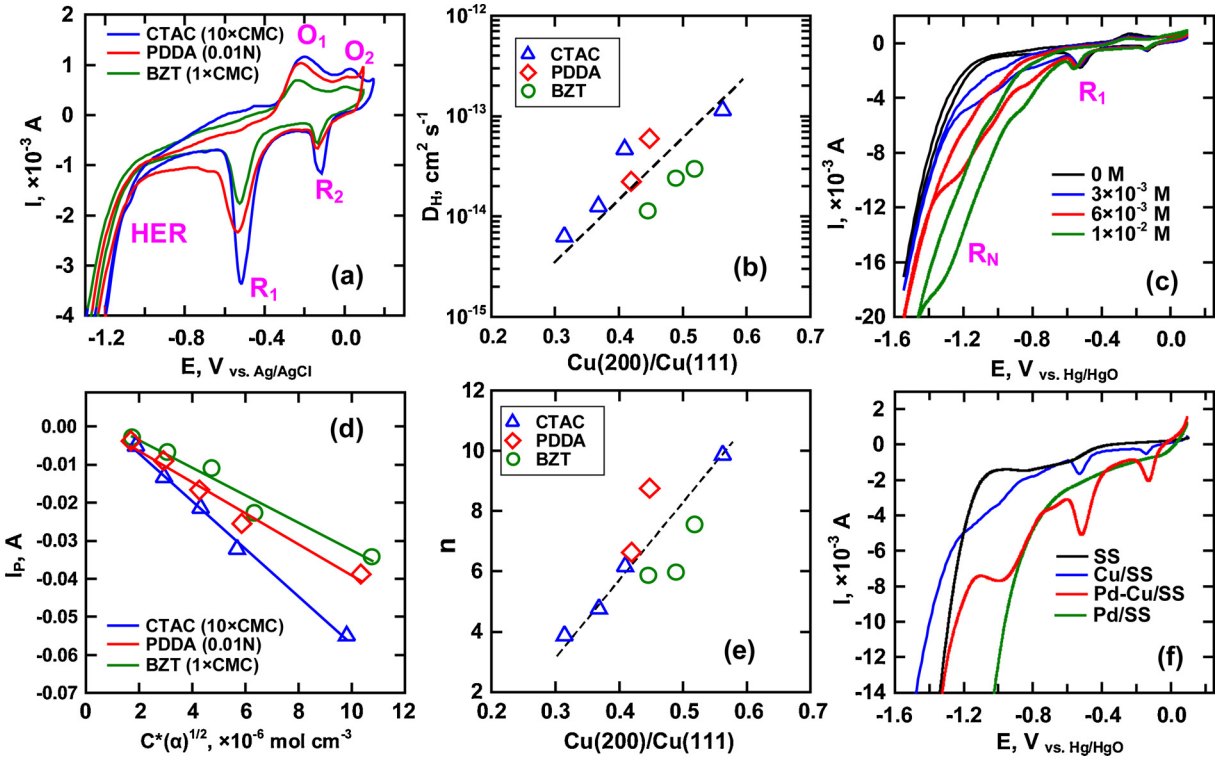

Fig. 4. Voltammetry analysis of surfactant-modified Cu/SS electrodes (a) in a supporting electrolyte of 0.1 M Na_2SO_4 (scan rate $=10\,mV\,s^{-1}$) and (b) D_H as a function of Cu(200)/Cu(111); (c) current-potential profile of solution containing 0 to 10^{-2} M KNO_3 (scan rate $=10\,mV\,s^{-1}$). (d) Linear regression of peak current for nitrate reduction versus the $C^*(\alpha)^{1/2}$, and (e) the correlation between the calculated electron number, n, transferred during NO_3- reduction as a function of area ratio of Cu(200)/Cu(111). (f) Voltammetry of stainless steel (SS), 1 × CMC BZT-modified Cu/SS and Pd-Cu/SS, and Pd/SS electrodes in the presence of 3 × 10^{-3} M KNO_3.

proportional to Cu(200)/Cu(111), which reflected the reactivity of Cu (200) and Cu(111) facets. Reduction of NO_3^- (+V) to nitrite (NO_2^-, +III) requires the transfer of two electrons. Further parallel reactions of nitrite to nitrogen gas (N_2, 0), and to ammonium ion (NH_4^+, -III) requires additional electrons greater than six [48]. Therefore, the ongoing reduction of nitrite may be sluggish on Cu(111), while the preference of Cu(200) benefits the yield of NH_4^+ at the lowest oxidation state.

Fig. 4f summarizes the voltammetry of cathodic polarization on electrodes in 3 × 10^{-3} M NO_3- solution. Although both the stainless steel (SS) support and Pd/SS (5 min plating time in $PdCl_2$ solution) showed no obvious peak current at R_N, H_2 evolution initiated at -0.8 V (vs. Hg/HgO) on Pd/SS, which was significantly increased respect to SS (at around -1.1 V). The independence of i-E with respect to KNO_3 concentration over Pd/SS (Fig. S7) was evidence that SS and Pd/SS were inactive in mediating electron transfer for NO_3- reduction. Fig. 4f shows that the peak potential decreased while peak current increased at R_N on Pd-Cu/SS electrode. Result indicated that Pd enriched the Cu electrode surface plentiful of hydrogen atoms for nitrate reduction.

3.3. Nitrate reduction on Cu/SS

Fig. 5 shows the electrochemical reduction of NO_3^- over surfactant-modified Cu/SS electrodes in solution containing 50 mg L^{-1} of initial NO_3^-N and 0.1 M of Na_2SO_4 as inert electrolyte as pH ~ 8.5 (uncontrolled). The temporary concentration of aqueous nitrogen species, namely, NO_3^-, NO_2^-, and NH_4^+ were measured at a constant current of 3 mA cm^{-2}. Other species such as NO and N_2O that potentially might evolve during electrolysis, were relatively unstable and could be rapidly transformed to N_2. Therefore, NO and N_2O were not considered in this work [49]. N_2 concentration was estimated from mass-balance relationship. Results show that generally, NO_3^- was mostly removed in 4 h. The concentrations of reaction products varied depending upon the type of Cu/SS electrodes prepared in electrolytes containing different types and concentrations of surfactants. Overall, NO_2^- and NH_4^+ were the two major byproducts. NO_2^- tended to evolve initially and declined when NH_4^+ and N_2 were generated with increasing electrolytic time; NO_2^- was an intermediate in a series of consecutive reaction and was being subsequently transformed to NH_4^+ or N_2, of which the selectivity was moderately dependent on the surfactant conditions. Fig. 6 shows results of classic Pearson analysis between S_N (%) (at 4 h) and Cu facet. S_{NO2-} and S_{NH4+} each exhibited negative and positive correlation to the Cu(200)/Cu(111) ratio, respectively, which were highly significant based on a two-tailed test (* denotes significance at 0.05 level). S_{NO2-} decreased from 70 to 30%, but S_{NH4+} improved from 20 to 60% in the Cu(200)/Cu(111) range of 0.3 to 0.6, confirming again the high reactivity of Cu(200). In contrast, S_{N2} and R(%), percent NO_3^- reduction, were less dependent on crystal property. Supposedly, the ordering plane of Cu metal did not affect the steps of direct nitrate reduction [28], however, the reactivity was determined by transferring electrons among the nitrogen species, which resulted in different conversion rate of NO_3^- to NO_2^- and to NH_4^+ [50,51]. Such finding also explained an inverse proportion between selective yields of NO_2^- and NH_4^+. (Note that when the intermediate NO_2^- starts to decrease after 100 min, more NH_4^+ keeps increasing than N_2 in Fig. 5).

3.4. Nitrate reduction on Pd-Cu/SS

Selectivity of nitrogen gas is maximized at around 25% by using 1 × CMC BZT-modified Cu/SS with a Cu(200)/Cu(111) facet ratio of 0.48, corresponding to 90% of NO_3^- removal (Fig. 5h); such Cu/SS was then applied to support the plating of Pd nanoparticulates. Characterization in Figs. 2 & 3 has indicated around 16.8% to 48.8% of Pd coated on the partially oxidized Cu_2O as increasing plating time in $PdCl_2$ solution from 1 min to 10 min. Fig. 7 presents the nitrate reduction over the Pd-Cu/SS electrodes, on which the efficiency of NO_3^- removal was all above 99% at 3 mA cm^{-2} in 4 h of electrolytic reaction.

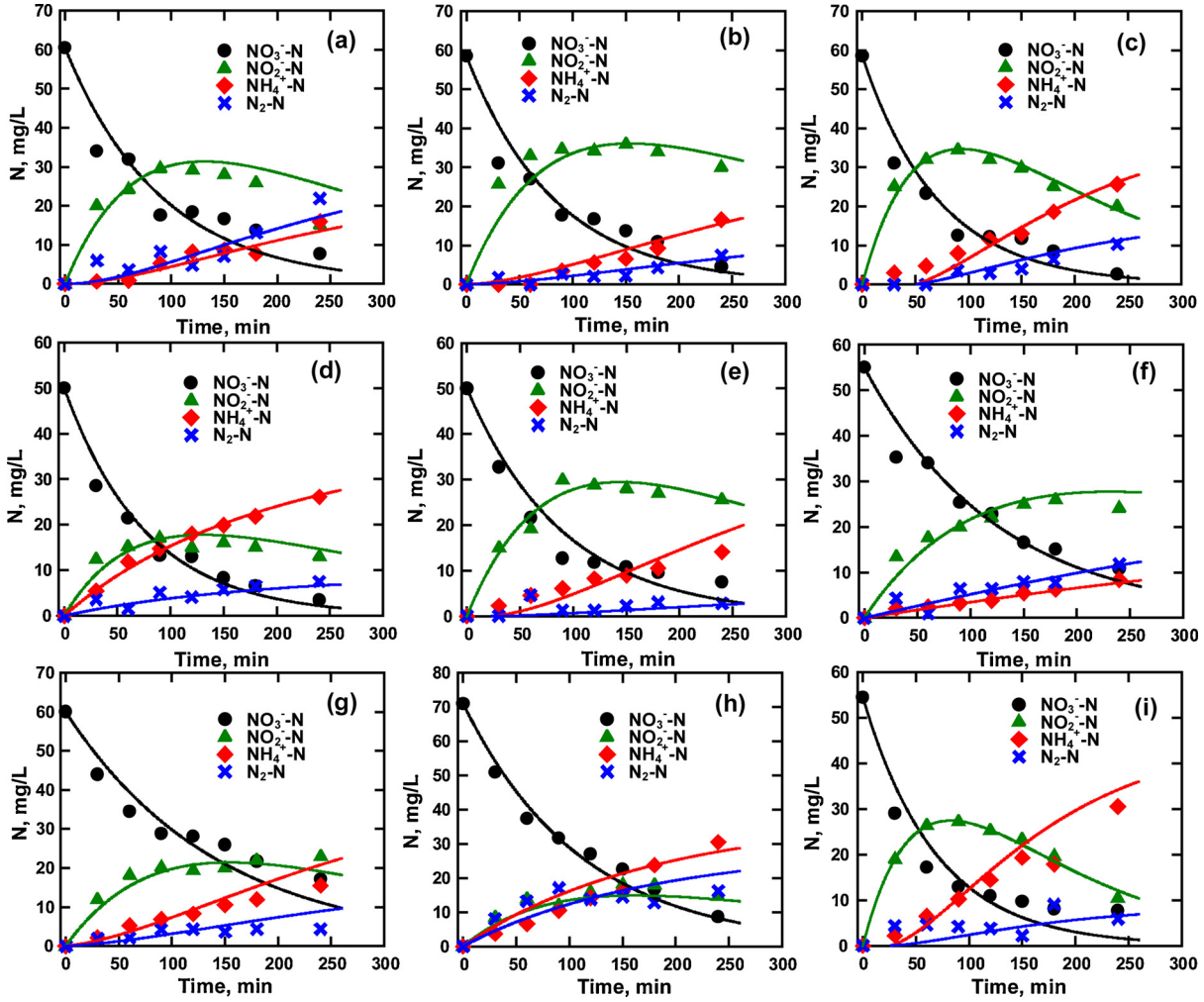

Fig. 5. Batch electrochemical reduction of nitrate (initial NO_3^- = 50 ~ 70 mg L^{-1}, 0.1 M Na_2SO_4, current density = 3 mA cm^{-2}, anode = IrO_2/Ti) over surfactant-modified Cu/SS electrodes with (a) 0.5 × CMC CTAC, (b) 1 × CMC CTAC, (c) 2 × CMC CTAC, (d) 10 × CMC CTAC, (e) 0.01 N, (f) 0.1 N PDDA, (g) 0.5 × CMC BZT, (h) 1 × CMC BZT, (i) 2 × CMC BZT.

Electrochemical reaction among nitrogen compounds over Pd-Cu/SS approached equilibrium in 100 min, which was much faster than those over Cu/SS. The concentration profiles suggested that intermediate NO_2^- formed in 50 min and almost disappeared afterward. NH_4^+ and N_2 were the two primary species on Pd-Cu/SS, in contrast to NO_2^- and NH_4^+ on Cu/SS. NO_2^- conversion to NH_4^+ was assumed to compete with that to N_2. Pd functioned as H-metal to induce indirect reduction because it did not contribute electrons to NO_3^- (evidenced by voltammetry in Fig. 4f and Fig. S7c), hence, NO_2^- was the product of the first electron step on Cu, and the precursor for hydrogenation on Pd as well. Furthermore, the ratio of Pd to Cu influenced the selectivity S_{N2}, which improved from 25% on Cu/SS (1 × CMC BZT) to 39.7%, 66.1%, and 49.6% on $Pd_{0.17}Cu_{0.82}$/SS, $Pd_{0.27}Cu_{0.73}$/SS, and $Pd_{0.49}Cu_{0.51}$/SS, respectively. As a result, Pd accelerated the conversion rate of nitrogen species in terms of indirect hydrogenation, while the Pd/Cu ratio should be optimized to improve the selectivity of either electrochemical or chemical reduction using H_2 as electron donor [52–54]. In the present work, a high yield of the nontoxic nitrogen gas was obtained on $Pd_{0.27}Cu_{0.73}$/SS.

3.5. Kinetics evaluation

The rate of NO_3^- reduction and evolution of NO_2^-, N_2, and NH_4^+ in aqueous solution were analyzed. The nitrate reduction was visualized as a hydrogenation process, by which the chemical reaction between the surface hydrogen and nitrogen species, on two different sites, occurred. Fig. 8 describes the electrode pathways, which begin with the adsorption of proton and nitrate on site S_1 (Pd) and S_2 (Cu), respectively:

$$S_1 + H^+ \rightleftharpoons S_1H^+ \quad (4)$$

$$S_2 + NO_3^- \rightleftharpoons S_2NO_3^-;\ K_1 \quad (5)$$

Cathodic polarization generates hydrogen radical and leads to hydrogen gas evolution:

$$S_1H^+ + e^- \longrightarrow S_1H \quad (6a)$$

$$2S_1H \longrightarrow S_1H_2 + S_1 + H_2 \quad (6b)$$

As mentioned above, Pd is primarily responsible for S_1 sites, which carry out the reactions of Eq. 6. Meanwhile, the first electron step that reduced nitrate to nitrite is carried on S_2 sites on Cu surface, i.e.,

$$S_2NO_3^- + 2S_1H^+ + 2e^- \longrightarrow S_2NO_2^- + S_1H_2O;\ k_2 \quad (7a)$$

$$S_2NO_2^- \rightleftharpoons S_2 + NO_2^-;\ K_3 \quad (7b)$$

The surface H, a strong reducing agent, then transfers electrons to the following nitrogen compounds.

$$S_2NO_2^- + 3S_1H \longrightarrow S_2N + S_1H_2O + S_1OH^-;\ k_4 \quad (8)$$

The N radical could be a critical reactant of the parallel reactions: 1) combination to form nitrogen gas (Eq. 9), or 2) successive

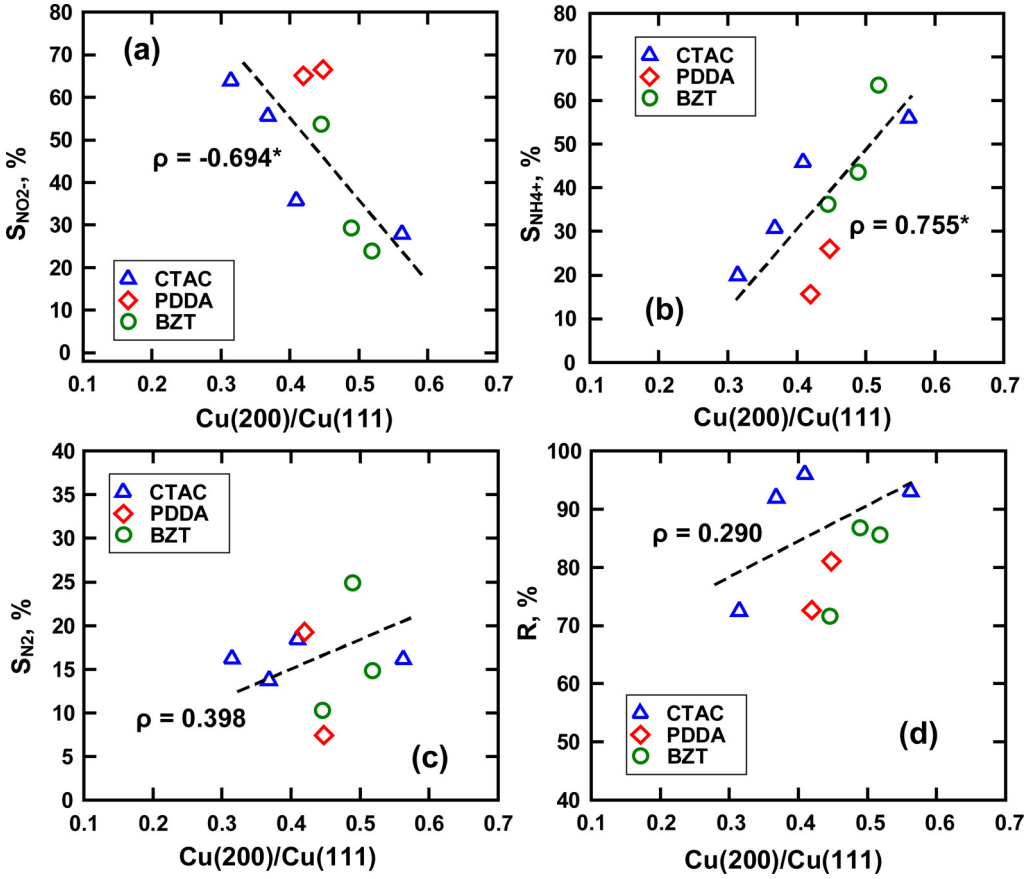

Fig. 6. Statistic analysis of Pearson correlation between the area ratio of Cu(200)/Cu(111) peaks and selectivity conversion of NO_3^--N to (a) NO_2^--N, (b) NH_4^+-N, and (c) N_2-N, and (d) efficiency of NO_3^- removal over the surfactant-modified Cu/SS electrodes. (* significance at 0.05 level in two-tailed test).

hydrogenation to produce ammonium ions (Eq. 10).

$$2S_2N \longrightarrow S_2N_2;\ k_5 \quad (9a)$$

$$S_2N_2 \rightleftharpoons S_2 + N_2;\ K_6 \quad (9b)$$

$$S_2N + 3S_1H \longrightarrow S_2NH_3;\ k_7 \quad (10a)$$

$$S_2NH_3 \rightleftharpoons S_2 + NH_3;\ K_8 \quad (10b)$$

$$NH_3 + H^+ \rightleftharpoons NH_4^+;\ K_a = 10^{9.25} \quad (10c)$$

By applying the steady-state approach, and assume that the concentration of all surface adsorbed species remains constant with time, i.e., adsorption rate equal to redox reaction rate. The concentration of free site is defined as a fractional surface coverage θ, and the sum of surface coverage, $\Sigma\theta_i$, of all active species, i.e., θ_H, θ_{NO3-}, θ_{NO2-}, θ_N, θ_{N2}, and θ_{NH3} is unity, i.e., $\Sigma\theta_i = 1$. The rate of steady-state species is listed in the following:

$$\frac{d\theta_{NO_3^-}}{dt} = k_1^+\theta[NO_3^-] - k_1^-\theta NO_3^- — k_2\theta_{NO_3^-}\theta_H^2[e]^2 = 0 \quad (11a)$$

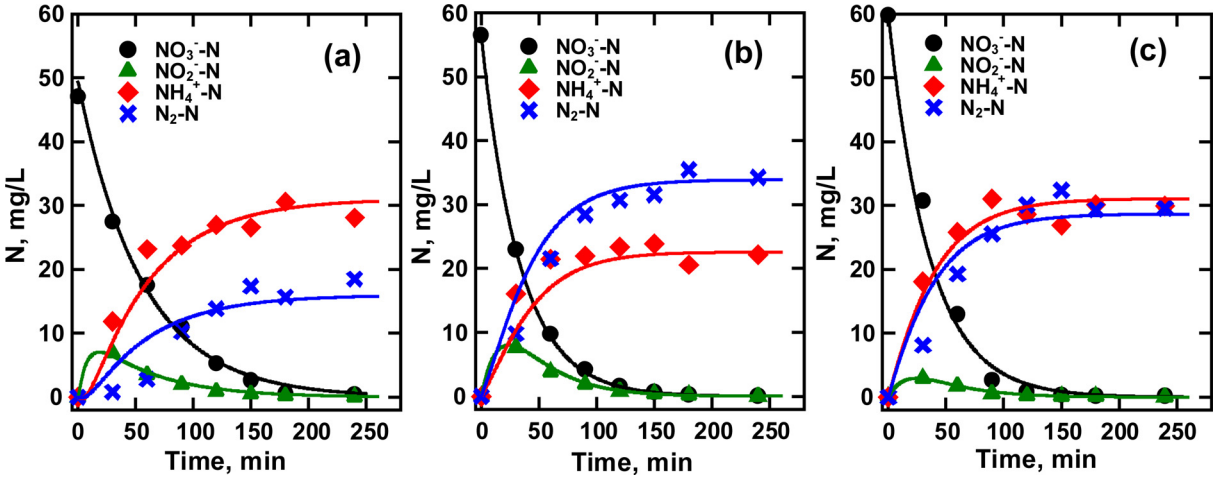

Fig. 7. Nitrate reduction and formation of nitrogen byproducts as a function of electrolytic time under constant current of 3 mA cm^{-2} (initial [NO_3^-N] = 50 ~ 60 mg L^{-1}; supporting electrolyte = 0.1 M Na_2SO_4, anode = IrO_2/Ti) over 1 × BZT modified (a) $Pd_{0.17}Cu_{0.82}$/SS, (b) $Pd_{0.27}Cu_{0.73}$/SS, and (c) $Pd_{0.49}Cu_{0.51}$/SS.

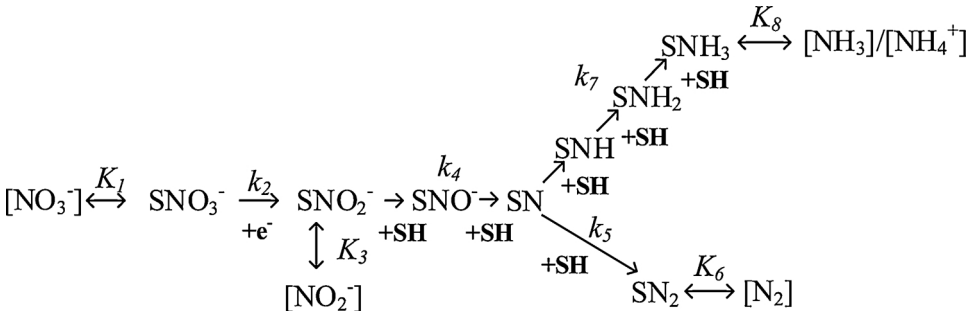

Fig. 8. Electrode pathway of nitrate hydrogenation and reduction.

$$\frac{d\theta_{NO_2^-}}{dt} = k_2\theta_{NO_3^-}\theta_H^2[e]^2 - k_3^+\theta_{NO_2^-} + k_3^-\theta[NO_2^-] - k_4\theta_{NO_2^-}\theta_H^3 = 0 \tag{11b}$$

$$\frac{d\theta_N}{dt} = k_4\theta_{NO_2^-}\theta_H^3 - 2k_5\theta_N - k_7\theta_N\theta_H^3 = 0 \tag{11c}$$

$$\frac{d\theta_{N_2}}{dt} = k_5\theta_N - k_6^+\theta_{N_2} + k_6^-\theta[N_2] = 0 \tag{11d}$$

$$\frac{d\theta_{NH_3}}{dt} = k_7\theta_N\theta_H^3 - k_8^+\theta_{NH_3} + k_8^-\theta[NH_3] = 0 \tag{11e}$$

Nitrogen compounds analyzed in solution are related to the rates of adsorption and desorption, and therefore to the rate of hydrogenation.

$$\frac{d[NO_3^-]}{dt} = -k_2\theta_{NO_3^-}\theta_H^2[e]^2 \tag{12a}$$

$$\frac{d[NO_2^-]}{dt} = k_2\theta_{NO_3^-}\theta_H^2[e]^2 - k_4\theta_{NO_2^-}\theta_H^3 \tag{12b}$$

$$\frac{d[N_2]}{dt} = k_6^+\theta_{N_2} - k_6^-\theta[N_2] = k_5\theta_N \tag{12c}$$

$$\frac{d[NH_3]}{dt} = k_7\theta_N\theta_H^3 \tag{12d}$$

Detail derivation of rate equations are given in Supporting Information. The concentration profile of relevant nitrogen species in the solution as a function of time can be obtained.

$$[NO_3^-] = [NO_3^-]_0 e^{-k_a t} \tag{13}$$

$$[NO_2^-] = \frac{k_a K_b}{k_c - k_a}[NO_3^-]_0(e^{-k_a t} - e^{-k_c t}) \tag{14}$$

$$[N_2] = \frac{2(k_c - k_a + k_a K_b)K_d}{k_c - k_a}[NO_3^-]_0(1 - e^{-k_a t}) - \frac{2k_a K_b K_d}{k_c - k_a}[NO_3^-]_0(1 - e^{-k_c t}) \tag{15}$$

$$[NH_3] = \frac{(k_c - k_a + k_a K_b)(1 - 2K_d)}{k_c - k_a}[NO_3^-]_0(1 - e^{-k_a t}) - \frac{k_a K_b(1 - 2K_d)}{k_c - k_a}[NO_3^-]_0(1 - e^{-k_c t}) \tag{16}$$

There are four constants computed as composite functions of rate constants in the reaction scheme (Fig. 8) from rate equations Eqs. 13–16, *i.e.*, $k_a = \frac{k_1^+ k_2\theta\theta_H^2[e]^2}{k_1^- + k_2\theta_H^2[e]^2}$, $K_b = \frac{k_3^+}{k_3^+ + k_4\theta_H^3}$, $k_c = \frac{k_3^- k_4\theta\theta_H^3}{k_3^+ + k_4\theta_H^3}$, and $K_d = \frac{k_5}{2k_5 + k_7\theta_H^3}$. Among the two rate constants, k_a is determined by the rate of adsorption (k_1^+) and the first electron step of direct reduction (k_2) of NO_3^-, and k_c is related to NO_2^- sorption (k_3-) and surface N formation (k_4). The other two constants, K_b describes the equilibrium of surface NO_2^- desorption (k_3^+) and hydrogenation (k_4); K_d reflects the competition between N_2 (k_5) and NH_4^+ (k_7) formation. In the presence of KNO_3, Cu is a mediator to directly transfer electrons for nitrogen reduction. The formation of nitrite strongly depends on an effective overpotential exhibited by the electrode. (Note that k_a is a function of [e].) On a monometallic Cu/SS electrode, when applying a constant current density to raise an electrode potential beyond the activation region, nitrogen is more efficiently reduced to its lowest oxidation state, i.e., NH_4^+, on Cu(200) than Cu(111) as revealed by voltammetry observation. For bimetallic system, Pd is the H-metal site which effectively captures H [55,56], resulted in a low hydrogen evolution overpotential (HEO) (as shown in Fig. 4f). The Pd site on Pd-Cu/SS played the essential role on promoting indirect hydrogenation of surface nitrite and nitrogen species, while the Cu site converts NO_3^- more to NO_2^- but less to NH_4^+, which aided the increase in N_2 yield.

Table S2 lists the rate constants obtained by fitting data in Figs. 5 and 7. Fig. 9a summaries the relationship between K_d and the facet ratio of Cu(200)/Cu(111). There was a clear trend towards higher N_2 selectivity (i.e., higher K_d) when Cu/SS had more Cu(111), even Cu^I(111) of Pd-Cu/SS. As the facet ratio of Cu(200)/Cu(111) dropped from 0.6 (60%) to 0.3 (30%), the K_d value, which was the rate ratio of N2 to that of the sum of N_2 and NH_4^+, increased from 0.1 (10%) to 0.3 (30%), indicating the essential role of Cu(111) in controlling the selectivity of nitrate reduction. Results of voltammetry (Fig. 4e) and batch electrolytic reaction (Fig. 6) suggested that Cu(200) was a highly reactive facet. High NH_4^+ yield was subject to low K_d since k_7 was large on Cu (200). Fig. 9b shows N_2 yield (the mass of N_2-N produced per unit mass of NO_3^--N) over all electrodes studied. As discussed above, for Cu/SS electrodes modified by different types of surfactants, the facet factor mainly affected the efficiency of Cu in mediating electron transfer for direct redox reactions. The selectivity of NO_2^- on Cu(111) was opposite to that of NH_4^+ on Cu(200), nonetheless, N_2 yield was low and less correlated to Cu facet. The average X_{N2} was in the range of 0.1 (10%) to 0.2(20%) on Cu/SS electrodes modified with surfactant. When prepared with 1 × CMC BZT as a modifier, the Cu/SS electrode exhibited the highest X_{N2} of 0.22(22%). Incorporating Pd, X_{N2} was enhanced up to 0.65 on $Pd_{0.27}Cu_{0.73}$/SS (5 min plating in $PdCl_2$ solution), proving the occurrence of effective hydrogenation on bimetallic electrodes.

Table 1 summaries the strategies of Cu-based electrodes preparation for NO_3^- removal. Methods applied to enhance the selective conversion to N_2 can be grouped into two categories: (1) bimetallic composites, such as Ni-Cu [57], Pd-Cu [47,58,59], Pt-Cu [29], Bi-Cu [60], and Sn-Cu [61]; (2) modification of Cu facet and morphology via plating. As showed in Fig. 4, Cu, an oxygen affinity (O) metal, also was an electron mediator that facilitated NO3- adsorption Incorporating H-affinity (H) metals, such as Pd, would accelerate hydrogenation of nitrogen intermediates. Note that hydrogen-affinity metals were also electron promoters. A specific ratio of O- to H-metal determined the production of NH_4^+ and N_2. However, N_2 yield was on the average below 40% over Cu-based catalyst because Cu was rather active in direct electron transfer, leading to high NO_3^- removal and high of NH_4^+ selectivity The effect of crystal facet of Cu moderately influenced the production of NO_2^- as a main intermediate, and Cu(111) was known to be less active than Cu(200) due to higher degree of passivation in Cu(111) [28,62]. In this work, the surfactant additive helped the elimination of NH_4^+ by

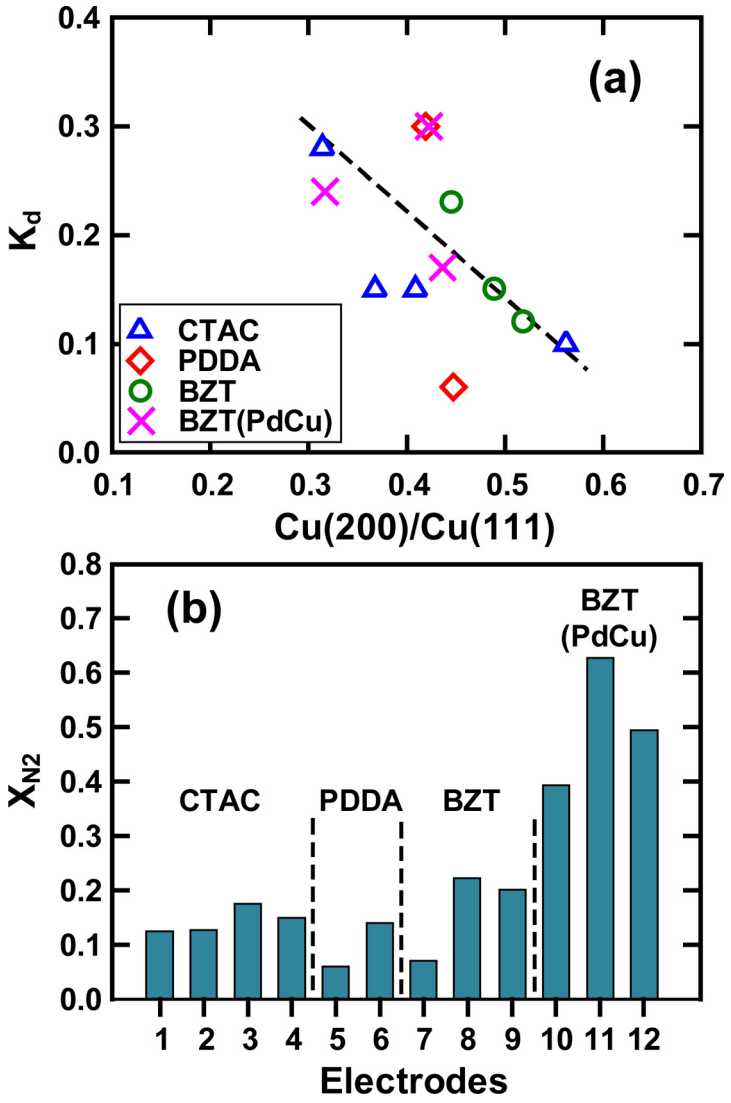

Fig. 9. (a) Correlation between equilibrium constant K_d of nitrate reduction and area ratio of (200)/(111) peaks of Cu.ss electrodes; (b) N_2-N yield (X_{N2}) from the nitrate reduction on surfactants-modified Cu/ss electrodes with (1) 0.5×, (2) 1×, (3) 2×, (4) 10 × CMC CTAC, (5) 0.01 N, (6) 0.1 N PDDA, (7) 0.5×, (8) 1×, (9) 2 × CMC BZT, and 1 × BZT modified Cu/ss electrodes with different Pd loading: (10) $Pd_{0.17}Cu_{0.83}$/SS, (11) $Pd_{0.27}Cu_{0.73}$/SS, and (12) $Pd_{0.49}Cu_{0.51}$/SS.

control of Cu(200)/Cu(111); hence, with Pd decoration, the hydrogenation of NO_2^-, derived from the first electron transferred to NO_3^- on Cu(111), could improve N_2 yield above 65%.

4. Conclusions

Morphological and crystallographic effects of copper metal on electrochemical nitrate reduction over Cu/SS and Pd-Cu/SS composite electrodes was investigated. Results of surface characterization using XRD and SEM revealed that the grain geometry and crystalline facet of Cu nanoparticles on stainless steel mesh support was properly established according to the type and concentration of surfactant additives (including CTAC, PDDA, and BZT). Cyclic voltammetry showed the onset potential NO_3^- reduction was more negative (or cathodic) that the Cu(0)/Cu(I) redox couple (< -0.6 V vs. Hg/HgO), which depicted the mechanism of direct NO_3^- reduction mediated by the phase transition of metallic Cu. The number of electron transferred among relevant nitrogen species increased over Cu/SS with preferentially phase oriented more toward Cu(200). Batch electrolysis of NO_3^- solution under constant current mode indicated the selectivity of NO_2^- being inversely proportional to that of NH_4^+, revealing the importance of Cu facet on byproduct formation; yet N_2 selectivity was low on single metallic Cu electrode (S_{N2} = 10–25 %). After the first electron step directly transferred via $Cu^{(0)}$, the subsequent reduction of NO_2^- and $N_{(ads)}$ that then dimerized to N_2, was effectively achieved on bimetallic Pd-Cu/SS. An optimal Pd:Cu at ratio of 0.27:0.73 substantially enhanced the N_2 yield to 0.65. Results of steady-state kinetics analysis revealed competition between N_2 and NH_4^+ formation which reaction rate was dependent on the area ratio of Cu(200)/Cu(111) peaks. Overall, Cu(111) enhanced rate of N_2 formation on Pd-Cu/SS electrode.

Declaration of interests

The authors declare that they have no known competing financial interests or personal relationships that could have appeared to influence the work reported in this paper.

CRediT authorship contribution statement

Yu-Jen Shih: Writing - original draft, Supervision. **Zhi-Lun Wu:** Resources. **Chun-Yen Lin:** Resources. **Yao-Hui Huang:** . **Chin-Pao Huang:** Conceptualization, Writing - review & editing.

Table 1
Strategy of fabricating Cu based electrode for electrochemical reduction of nitrate.

Electrodes	Strategy and key findings	Efficiency	Ref.
$Pd_{40}Cu_{60}$/SS	Electrodeposition of Cu and Pd-Cu was developed to study the kinetics of nitrate hydrogenation.	Selectivity to N_2 = 40%, electrode potential = -0.3 V, 50 mg/L NO_3-N, pH 7	[47]
$Pd_{20}Cu_{80}$/Cu $Ni_{20}Cu_{80}$/Cu	X-Cu alley (X = Ni, Fe, Pd, Pb) electrodes prepared by ball milling were used to study effect of composite metals.	Selectivity to N_2 = 39% for $Pd_{20}Cu_{80}$; 37% for $Ni_{20}Cu_{80}$ at NaOH = 1 M, NO_3-N = 0.1 M	[57]
$Pd_{80}Cu_{20}$/NiAl	Electrosorption of NO_3^- on layer metal oxide significantly improved reduction of NO_3^- by Pd-Cu coating	Sorption of NO_3-N achieved 2 mg/g at potential of 1.0 V, final removal rate = 61.8%	[58]
Pd_5Cu_{95}/Cu	Pd/Al_2O_3 pellets was bound on Cu plate using polyester as binder	NO_3^- removal = 59%, selectivity to N_2 = 35% at NO_3-N = 135 mg/L, current density = 1.1 mA/cm^2	[59]
$Bi_{10}Cu_{90}$/Cu	Bi element was deposited onto pure Cu sheets by electroplating.	NO_3^- removal = 87.5% at NO_3-N = 100 mg/L, current density = 6 mA/cm^2	[60]
Pt-Cu/NF, Pd-Cu/NF	Pt and Pd nanoparticles were deposited on Nafion (NF) membrane via $NaBH_4$ reduction, and Cu was electrochemically coated onto Pt or Pd surfaces at DC current of 50 mA	The continuous flow rate influence the selective conversion which are 24% and 14% for NH_4^+ and NO_2^- at 0.1 mL/min. NO_3^- removal = 93% at NO_3-N = 45 mg/L, current density = 0.1 A.	[29]
Sn-Cu/Pt-NF	Electrodeposition of Cu and SnCu loaded on Pt Nafion memebrane; Pt-H provided a reducing environment	The selective conversion for NH_4^+ and NO_2^- are 39% and 44% over Cu-Pt at NO_3-N = 0.05 M, current density = 0.1 A. Sn significantly enhanced the selectivity of molecular nitrogen	[61]
Single Cu crystal	Activity between Cu(100), Cu(110), and Cu(111) discs via shell isolated nanoparticle enhanced Raman spectroscopy (SHINERS)	All planes have the same mechanism in nitrate reduction, while Cu (111) and Cu(110) are more susceptible to oxidation; nitrate showed higher adsorption energy on Cu_2O(111)	[62]
Cu/Ni	Cu facet was varied by electrodeless deposition time on Ni substrate using tartrate as chelating agent.	Shorter plating time resulted in more Cu_2O(111) oriented, improving the selectivity of N_2 (33%) and nitrate removal (97%) at NO_3-N = 50 mg/L, current density = 3 mA/cm^2	[28]
Cu/SS and Pd-Cu/SS	Cu facets in (111) and (200) were adjusted with the aid of surfactant during electrodeposition on stainless steel mesh; Pd loading amount was critical to indirect hydrogenation	Cu(111) retarded the formation of NH_4^+ over 1 × CMC BZT modified Cu/SS. After incorporated with Pd, N_2 yield significantly increased up to 65% at NO_3-N = 50 mg/L, current density = 3 mA/cm^2.	Present work

Acknowledgement

The authors would like to thank the Ministry of Science and Technology, Taiwan for generous finance support of this research under Contract No. MOST 108-2628-E-110-005-MY3. Addition support was provided by US NSF IOA (1632899) to CPH.

Appendix A. Supplementary data

Supplementary material related to this article can be found, in the online version, at doi:https://doi.org/10.1016/j.apcatb.2020.119053.

References

[1] M. Gutiérrez, R.N. Biagioni, M.T. Alarcón-Herrera, B.A. Rivas-Lucero, An overview of nitrate sources and operating processes in arid and semiarid aquifer systems, Sci. Total Environ. 624 (2018) 1513–1522, https://doi.org/10.1016/j.scitotenv.2017.12.252.
[2] J. Martínez, A. Ortiz, I. Ortiz, State-of-the-art and perspectives of the catalytic and electrocatalytic reduction of aqueous nitrates, Appl. Catal. B Environ. 207 (2017) 42–59, https://doi.org/10.1016/j.apcatb.2017.02.016.
[3] L. Calvo, M.A. Gilarranz, J.A. Casas, A.F. Mohedano, J.J. Rodriguez, Denitrification of water with activated carbon-supported metallic catalysts, Ind. Eng. Chem. Res. 49 (2010) 5603–5609, https://doi.org/10.1021/ie100838r.
[4] A. Bhatnagar, M. Sillanpää, A review of emerging adsorbents for nitrate removal from water, Chem. Eng. J. 168 (2011) 493–504, https://doi.org/10.1016/j.cej.2011.01.103.
[5] R.R. Karri, J.N. Sahu, V. Chimmiri, Critical review of abatement of ammonia from wastewater, J. Mol. Liq. 261 (2018) 21–31, https://doi.org/10.1016/j.molliq.2018.03.120.
[6] S. Ghafari, M. Hasan, M.K. Aroua, Bio-electrochemical removal of nitrate from water and wastewater—a review, Bioresour. Technol. 99 (2008) 3965–3974, https://doi.org/10.1016/j.biortech.2007.05.026.
[7] S. Mousavi, S. Ibrahim, M. Kheireddine, A.S. Ghafari, Development of nitrate elimination by autohydrogenotrophic bacteria in bio-electrochemical reactors—a review, Biochem. Eng. J. 67 (2012) 251–264, https://doi.org/10.1016/j.bej.2012.04.016.
[8] S. Sevda, T.R. Sreekishnan, N. Pous, S. Puig, D. Pant, Bioelectroremediation of perchlorate and nitrate contaminated water: a review, Bioresour. Technol. 255 (2018) 331–339, https://doi.org/10.1016/j.biortech.2018.02.005.
[9] M.O. Rivett, S.R. Buss, P. Morgan, J.W.N. Smith, C.D. Bemment, Nitrate attenuation in groundwater: a review of biogeochemical controlling processes, Water Res. 42 (2008) 4215–4232, https://doi.org/10.1016/j.watres.2008.07.020.
[10] M.A. Hasnat, M.A. Islam, S.B. Aoun, J.A. Safwan, M.M. Rahman, A.M. Asiri, Composite noble-metal films/H^+ -conducting solid-polymer electrolyte assemblies: the nitrate-reduction activity in an asymmetric sandwich-type reactor, Chempluschem 80 (11) (2015) 1634–1641, https://doi.org/10.1002/cplu.201500255.
[11] M.R. Awual, M.M. Hasan, A.M. Asiri, M.M. Rahman, Cleaning the arsenic(V) contaminated water for safe-guarding the public health using novel composite material, Compos. B Eng. 171 (2019) 294–301, https://doi.org/10.1016/j.compositesb.2019.05.078.
[12] M.A. Hasnat, Z. Mumtarin, M.M. Rahman, Electrocatalytic reduction of hydroxylamine on copper immobilized platinum surface: heterogeneous kinetics and sensing performance, Electrochim. Acta 318 (2019) 486–495, https://doi.org/10.1016/j.electacta.2019.06.058.
[13] M.M. Alam, A.M. Asiri, M.T. Uddin, M.A. Islam, M.R. Awual, M.M. Rahman, Detection of uric acid based on doped $ZnO/Ag_2O/Co_3O_4$ nanoparticle loaded glassy carbon electrode, New J. Chem. 43 (2019) 8651–8659, https://doi.org/10.1039/C9NJ01287G.
[14] G. Maduraiveeran, M. Sasidharan, W. Jin, Earth-abundant transition metal and metal oxide nanomaterials: synthesis and electrochemical applications, Prog. Mater. Sci. 106 (2019) 100574, https://doi.org/10.1016/j.pmatsci.2019.100574.
[15] O.M. Cornejo, M.F. Murrieta, L.F. Castañeda, J.L. Nava, Characterization of the reaction environment in flow reactors fitted with BDD electrodes for use in electrochemical advanced oxidation processes: a critical review, Electrochim. Acta 331 (2020) 135373, https://doi.org/10.1016/j.electacta.2019.135373.
[16] S. Jung, S. Bae, W. Lee, Development of Pd−Cu/Hematite catalyst for selective nitrate reduction, Environ. Sci. Technol. 48 (2014) 9651–9658, https://doi.org/10.1021/es502263p.
[17] F. Yao, Q. Yang, Y. Zhong, X. Shu, F. Chen, J. Sun, Y. Ma, Z. Fu, D. Wang, X. Li, Indirect electrochemical reduction of nitrate in water using zero-valent titanium anode: factors, kinetics, and mechanism, Water Res. 157 (2019) 191–200, https://doi.org/10.1016/j.watres.2019.03.078.
[18] Y. Liu, J. Wang, Reduction of nitrate by zero valent iron (ZVI)-based materials: a review, Sci. Total Environ. 671 (2019) 388–403, https://doi.org/10.1016/j.scitotenv.2019.03.317.
[19] G. Tokazhanov, E. Ramazanova, S. Hamid, S. Bae, W. Lee, Advances in the catalytic reduction of nitrate by metallic catalysts for high efficiency and N_2 selectivity: a review, Chem. Eng. J. 384 (2020) 123252, https://doi.org/10.1016/j.cej.2019.123252.
[20] M.M. Alam, M.A. Hasnat, M.A. Rashed, S.M.N. Uddin, M.M. Rahman, S. Amertharaj, N. Ahmed, N. Mohamed, Nitrate detection activity of Cu particles deposited on pencil graphite by fast scan cyclic voltammetry, J. Anal. Chem. 70 (2015) 60–66, https://doi.org/10.1134/S1061934815010037.
[21] F. Yu, T. Huang, P. Zhang, Y. Tao, F.Z. Cui, Q. Xie, S. Yao, F. Wang, Design and synthesis of electrode materials with both battery-type and capacitive charge storage, Energy Storage Mater. 22 (2019) 235–255, https://doi.org/10.1016/j.ensm.2019.07.023.
[22] M.R. Ehrenburg, A.I. Danilov, I.G. Botryakova, E.B. Molodkina, A.V. Rudnev, Electroreduction of nitrate anions on cubic and polyoriented platinum nanoparticles modified by copper adatoms, J. Electroanal. Chem. 802 (2017) 109–117, https://doi.org/10.1016/j.jelechem.2017.08.051.
[23] D.F. Zhang, H. Zhang, L. Guo, K. Zheng, X.D. Han, Z. Zhang, Delicate control of crystallographic facet-oriented Cu_2O nanocrystals and the correlated adsorption ability, J. Mater. Chem. 19 (2009) 5220–5225, https://doi.org/10.1039/B816349A.
[24] C.H. Kuo, Y.C. Yang, S. Gwo, M.H. Huang, Facet-dependent and Au nanocrystal-

enhanced electrical and photocatalytic properties of Au-Cu_2O core-shell heterostructures, J. Am. Chem. Soc. 133 (2011) 1052–1057, https://doi.org/10.1021/ja109182y.
[25] Y. Su, H. Li, H. Ma, J. Robertson, A. Nathan, Controlling surface termination and facet orientation in Cu_2O nanoparticles for high photocatalytic activity: a combined experimental and density functional theory study, ACS Appl. Mater. Interfaces 9 (2017) 8100–8106, https://doi.org/10.1021/acsami.6b15648.
[26] S. Sun, X. Zhang, Q. Yang, S. Liang, X. Zhang, Z. Yang, Cuprous oxide (Cu_2O) crystals with tailored architectures: a comprehensive review on synthesis, fundamental properties, functional modifications and applications, Prog. Mater. Sci. 96 (2018) 111–173, https://doi.org/10.1016/j.pmatsci.2018.03.006.
[27] D. Zhang, B. Wang, X. Gong, Z. Yang, Y. Liu, Selective reduction of nitrate to nitrogen gas by novel Cu_2O-Cu°@Fe° composite combined with HCOOH under UV radiation, Chem. Eng. J. 359 (2019) 1195–1204, https://doi.org/10.1016/j.cej.2018.11.058.
[28] Y.J. Shih, Z.L. Wu, Y.H. Huang, C.P. Huang, Electrochemical nitrate reduction as affected by the crystal morphology and facet of copper nanoparticles supported on nickel foam electrodes (Cu/Ni), Chem. Eng. J. 383 (2020) 123157, https://doi.org/10.1016/j.cej.2019.123157.
[29] M.A. Hasnat, S.B. Aoun, M.M. Rahman, A.M. Asiri, N. Mohamed, Lean Cu-immobilized Pt and Pd films/-H^+ conducting membrane assemblies: relative electrocatalytic nitrate reduction activities, J. Ind. Eng. Chem. 28 (2015) 131–137, https://doi.org/10.1016/j.jiec.2015.02.008.
[30] K. Shimazu, R. Goto, S. Piao, R. Kayama, K. Nakata, Y. Yoshinaga, Reduction of nitrate ions on tin-modified palladium thin film electrodes, J. Electroanal. Chem. 601 (2007) 161–168, https://doi.org/10.1016/j.jelechem.2006.11.005.
[31] M. Kato, M. Okui, S. Taguchi, I. Yagi, Electrocatalytic nitrate reduction on well-defined surfaces of tin-modified platinum, palladium and platinum-palladium single crystalline electrodes in acidic and neutral media, J. Electroanal. Chem. 800 (2017) 46–53, https://doi.org/10.1016/j.jelechem.2017.01.020.
[32] J.F. Su, W.F. Kuan, H. Liu, C.P. Huang, Mode of electrochemical deposition on the structure and morphology of bimetallic electrodes and its effect on nitrate reduction toward nitrogen selectivity, Appl. Catal. B Environ. 257 (2019) 117909, https://doi.org/10.1016/j.apcatb.2019.117909.
[33] C. Breinlich, J. Haubrich, C. Becker, A. Valcárcel, F. Delbecq, K. Wandelt, Hydrogenation of 1,3-butadiene on Pd(111) and PdSn/Pd(111) surface alloys under UHV conditions, J. Catal. 251 (2007) 123–130, https://doi.org/10.1016/j.jcat.2007.07.003.
[34] O.S.G.P. Soares, J.J.M. Órfão, M.F.R. Pereira, Nitrate reduction with hydrogen in the presence of physical mixtures with mono and bimetallic catalysts and ions in solution, Appl. Catal. B Environ. 102 (2011) 424–432, https://doi.org/10.1016/j.apcatb.2010.12.017.
[35] M.M. Hossain, K. Nakata, T. Kawaguchi, K. Shimazu, Reduction of nitrate on electrochemically pre-reduced tin-modified palladium electrodes, J. Electroanal. Chem. 707 (2013) 59–65, https://doi.org/10.1016/j.jelechem.2013.08.015.
[36] K.A. Resende, C.A. Teles, G. Jacobs, B.H. Davis, D.C. Cronauer, A.J. Kropff, C.L. Marshallf, C.E. Horia, F.B. Noronha, Hydrodeoxygenation of phenol over zirconia supported Pd bimetallic catalysts. The effect of second metal on catalyst performance, Appl. Catal. B Environ. 232 (2018) 213–231, https://doi.org/10.1016/j.apcatb.2018.03.041.
[37] C. Pignolet, M. Euvrard, A. Foissy, C. Filiâtre, Electrodeposition of latex particles in the presence of surfactant: investigation of deposit morphology, J. Colloid Interface Sci. 349 (2010) 41–48, https://doi.org/10.1016/j.jcis.2010.05.004.
[38] T.R. Gordon, M. Cargnello, T. Paik, F. Mangolini, R.T. Weber, P. Fornasiero, C.B. Murray, Nonaqueous synthesis of TiO_2 Nanocrystals using TiF_4 to engineer morphology, oxygen vacancy concentration, and photocatalytic activity, J. Am. Chem. Soc. 134 (2012) 6751–6761, https://doi.org/10.1021/ja300823a.
[39] S. Kobayashi, D.A. Tryk, H. Uchida, Enhancement of hydrogen evolution activity on Pt-skin/Pt_3Co [(111), (100), and (110)] single crystal electrodes, Electrochem. Comm. 110 (2020) 106615, https://doi.org/10.1016/j.elecom.2019.106615.
[40] M.C. Biesinger, Advanced analysis of copper X-ray photoelectron spectra, Surf. Interface Anal. 49 (2017) 1325–1334, https://doi.org/10.1002/sia.6239.
[41] M.A. Hasnat, M.M. Rahman, I.A. Siddiquey, S.M. Borhanuddin, M.S. Alam, M.H. Rahman, A.M. Asiri, Aggregated Pt-Pd nanoparticles on Nafion membrane for impulsive decomposition of hydrogen peroxide, RSC Adv. 5 (2015) 46295, https://doi.org/10.1039/C5RA05620A.
[42] J.X. Tang, Q.S. Chen, L.X. You, H.G. Liao, S.G. Sun, S.G. Zhou, Z.N. Xu, Y.M. Chen, G.C. Guo, Screw-like PdPt nanowires as highly efficient electrocatalysts for methanol and ethylene glycol oxidation, J. Mater. Chem. A 6 (5) (2018) 2327–2336, https://doi.org/10.1039/C7TA09595C.
[43] J.M. Lee, K.K. Jung, J.S. Ko, Growth mechanism and application of nanostructures fabricated by a copper sulfate solution containing boric acid, J. Electrochem. Soc. 163 (8) (2016) D407–D413, https://doi.org/10.1149/2.0691608jes.
[44] M.M. Alam, M.A. Rashed, M.M. Rahman, M.M. Rahman, Y. Nagao, M.A. Hasnat, Electrochemical oxidation of As(III) on Pd immobilized Pt surface: kinetics and sensing performance, RSC Adv. 8 (2018) 8071, https://doi.org/10.1039/C7RA12576C.
[45] Z. Wang, G. Yang, Z. Zhang, M. Jin, Y. Yin, Selectivity on etching: creation of high-energy facets on copper nanocrystals for CO_2 electrochemical reduction, ACS Nano 10 (2016) 4559–4564, https://doi.org/10.1021/acsnano.6b00602.
[46] C. Picioreanu, M.C.M. van Loosdrecht, J.J. Heijnen, Modelling the effect of oxygen concentration on nitrite accumulation in a biofilm airlift suspension reactor, Water Sci. Technol. 36 (1) (1997) 147–156, https://doi.org/10.1016/S0273-1223(97)00347-8.
[47] J.F. Su, I. Ruzybayev, I. Shah, C.P. Huang, The electrochemical reduction of nitrate over micro-architectured metal electrodes with stainless steel scaffold, Appl. Catal. B Environ. 180 (2016) 199–209, https://doi.org/10.1016/j.apcatb.2015.06.028.
[48] D. Reyter, D. Bélanger, L. Roué, Study of the electroreduction of nitrate on copper in alkaline solution, Electrochim. Acta 53 (2008) 5977–5984, https://doi.org/10.1016/j.electacta.2008.03.048.
[49] E. Pérez-Gallent, M.C. Figueiredo, I. Katsounaros, M.T.M. Koper, Electrocatalytic reduction of nitrate on copper single crystals in acidic and alkaline solutions, Electrochim. Acta 227 (2017) 77–84, https://doi.org/10.1016/j.electacta.2016.12.147.
[50] G.E. Badea, Electrocatalytic reduction of nitrate on copper electrode in alkaline solution, Electrochim. Acta 54 (2009) 996–1001, https://doi.org/10.1016/j.electacta.2016.12.147.
[51] D. Yin, Y. Liu, P. Song, P. Chen, X. Liu, L. Cai, L. Zhang, In situ growth of copper/reduced graphene oxide on graphite surfaces for the electrocatalytic reduction of nitrate, Electrochim. Acta 324 (2019) 134846, https://doi.org/10.1016/j.electacta.2019.134846.
[52] Y. Yoshinaga, T. Akita, I. Mikami, T. Okuhara, Hydrogenation of nitrate in water to nitrogen over Pd-Cu supported on active carbon, J. Catal. 207 (2002) 37–45, https://doi.org/10.1006/jcat.2002.3529.
[53] Q. Zhang, L. Ding, H. Cui, J. Zhai, Z. Wei, Q. Li, Electrodeposition of Cu-Pd alloys onto electrophoretic deposited carbon nanotubes for nitrate electroreduction, Appl. Surf. Sci. 308 (2014) 113–120, https://doi.org/10.1016/j.apsusc.2014.04.119.
[54] L. Mattarozzi, S. Cattarin, N. Comisso, R. Gerbasi, P. Guerriero, M. Musiani, E. Verlato, Electrodeposition of compact and porous Cu-Pd alloy layers and their application to nitrate reduction in alkali, Electrochim. Acta 230 (2017) 365–372, https://doi.org/10.1016/j.electacta.2017.02.012.
[55] H. Duncan, A. Lasia, Separation of hydrogen adsorption and absorption on Pd thin films, Electrochim. Acta 53 (2008) 6845–6850, https://doi.org/10.1016/j.electacta.2007.12.012.
[56] B.P. Chapli, M. Reinhard, W.F. Schneider, C. Schüth, J.R. Shapley, T.J. Strathmann, C.J. Werth, Critical review of Pd-based catalytic treatment of priority contaminants in water, Environ. Sci. Technol. 46 (7) (2012) 3655–3670, https://doi.org/10.1021/es3031648.
[57] L. Li, Y. Yun, Y. Zhang, Y. Huang, Z. Xu, Electrolytic reduction of nitrate on copper and its binary composite electrodes, J. Alloys Compd. 766 (2018) 157–160, https://doi.org/10.1016/j.jallcom.2018.07.004.
[58] Z. Bai, J. Dong, G. Liu, T.T.I. Nkambule, C. Hu, J. Qu, Denitrification enhancement by electro-sorption/reduction using a layered metal oxide electrode loaded with Pd-Cu nanoparticles, Electrochem. Commun. 110 (2020) 106607, https://doi.org/10.1016/j.elecom.2019.106607.
[59] T.F. Beltrame, M.C. Gomes, L. Marder, F.A. Marchesini, M.A. Ulla, A.M. Bernardes, Use of copper plate electrode and Pd catalyst to the nitrate reduction in an electrochemical dual-chamber cell, J. Water Proc. Eng. 35 (2020) 101189, https://doi.org/10.1016/j.jwpe.2020.101189.
[60] W. Gao, L. Gao, D. Li, K. Huang, L. Cui, J. Meng, J. Liang, Removal of nitrate from water by the electrocatalytic denitrification on the Cu-Bi electrode, J. Electroanal. Chem. 817 (2018) 202–209, https://doi.org/10.1016/j.jelechem.2018.04.006.
[61] P.P. Koay, M.S. Alam, M.M. Alam, M. Etesami, M.A. Hasnat, N. Mohamed, Electrocatalytic reduction of nitrate ions at a poly crystalline SnCu modified platinum surface by using an H^+ conducting solid polymer in a sandwich type membrane reactor, J. Environ. Chem. Eng. 4 (2016) 4494–4502, https://doi.org/10.1016/j.jece.2016.10.004.
[62] D.P. Butcher Jr., A.A. Gewirth, Nitrate reduction pathways on Cu single crystal surfaces: effect of oxide and Cl^-, Nano Energy 29 (2016) 457–465, https://doi.org/10.1016/j.nanoen.2016.06.024.